SCIENCE CHINA
Technological Sciences

March 2013 Vol.56 No.3: 713–723
doi: 10.1007/s11431-012-5109-x

Uncertainty analysis of cross-calibration for HJ-1 CCD camera

WANG Zuo[1,2], XIAO PengFeng[1,2*], GU XingFa[3], FENG XueZhi[1,2], LI XiaoYing[3], GAO HaiLiang[3], LI Hui[4,2], LIN JinTang[5,2] & ZHANG XueLiang[1,2]

[1] *Jiangsu Provincial Key Laboratory of Geographic Information Science and Technology, Nanjing University, Nanjing 210093, China;*
[2] *Department of Geographic Information Science, Nanjing University, Nanjing 210093, China;*
[3] *State Key Laboratory of Remote Sensing Science, Jointly Sponsored by the Institute of Remote Sensing Applications of Chinese Academy of Sciences and Beijing Normal University, Beijing 100101, China;*
[4] *Department of Spatial Information Science and Engineering, Xiamen University of Technology, Xiamen 361024, China;*
[5] *Department of Geography Science, Minjiang University, Fuzhou 350108, China*

Received July 12, 2012; accepted December 18, 2012; published online January 10, 2013

Radiometric calibration of sensor is the basis of quantitative remote sensing, and uncertainty analysis is critical to ensure the accuracy of cross-calibration. Therefore, firstly, cross-calibration formulas were improved by redefining calibration coefficient and spectral band matching factor. In these formulas, c_{ci} was redefined as the calibration coefficient of normalized apparent reflectance, and spectral band matching factor as the ratio of normalized apparent reflectance. Secondly, based on the contrast of ideal and actual conditions in cross-calibration, 8 sources of cross-calibration uncertainty were proposed: calibration uncertainty of standard sensor; pixel matching uncertainty; spectral band matching factor uncertainty caused by site altitude setting error, atmospheric parameters setting error, surface spectrum source, surface bidirectional reflectance characteristic, and error of atmospheric radiative transfer model; and uncertainty caused by other factors which were not considered. Finally, the contribution of each uncertainty was further analyzed and discussed for the HJ-1 CCD camera. The results provide many valuable references for evaluating the feasibility of alternative cross-calibration measurements.

cross-calibration, uncertainty analysis, CCD camera, HJ-1

Citation: Wang Z, Xiao P F, Gu X F, et al. Uncertainty analysis of cross-calibration for HJ-1 CCD camera. Sci China Tech Sci, 2013, 56: 713–723, doi: 10.1007/s11431-012-5109-x

1 Introduction

HJ-1 is the first small satellite constellation in China designed for environment and disaster monitoring. Since it was launched successfully on September 6, 2008, a great amount of images of China and surrounding areas have been provided for environmental monitoring, disaster prevention and mitigation. Absolute radiometric calibration is the basis of quantitative remote sensing. In order to promote the quantitative application of the data, high precision and high frequency calibration for HJ-1 CCD camera is necessary. Cross-calibration is a very common method of radiometric calibration, due to its simple operation and low cost. It has great significance in making up for the deficiency of single calibration method, developing multi-method comparative application, and finally improving the calibration accuracy.

In general, as one of the supplements for spaceborne calibration, cross-calibration is used for cross-validation with spaceborne calibration and vicarious calibration. In addition, time series cross-calibrations are often performed to monitor the sensor's attenuation. Many satellite sensors have carried

*Corresponding author (email: xiaopf@gmail.com)

out cross-calibration, such as NOAA/AVHRR [1, 2], SPOT/VEGETATION [3], SPOT/HRVIR [3], Landsat-5/TM [4, 5], Terra/MODIS [6–8], MIR-Station/MOMS [9], OrbView-2/SeaWiFS [6, 10], and ADEOS/POLDER [7, 11]. In China, there are also many scientists engaged in the cross-calibration research, and realized cross-calibration for many domestic remote sensors, such as CBERS/CCD [12–14], CBERS/WFI [13], BJ-1/CCD [15], SZ-3/CMODIS [16, 17], FY-1D/VIRR [16], HJ-1/CCD [18–20], and HY-1A/COCTS [21].

Uncertainty analysis is the key step for cross-calibration. It affects the choice of alternative measurements and the accuracy of calibration. A large number of researches about it have been developed [7, 13, 18, 22], but there are less theoretical derivation and rounded analysis for cross-calibration uncertainty sources and their influence mechanism. In this paper, uncertainty sources were inferred based on the cross-calibration principle and the comparison of ideal and actual conditions in cross-calibration, and then the contribution of each uncertainty was further analyzed, thus providing many valuable references for the selection of alternative cross-calibration measurements.

2 Principle

The optical sensor cross-calibration is to use a high precision calibrated standard sensor to calibrate the target sensor and thereby obtain the calibration coefficients. In this procedure, it needs firstly to obtain the digital count values from the images, match their spectral responses, observation geometries and atmospheric parameters, then establish the relationship between the digital count values and calibration coefficients of the two sensors, and finally calculate calibration coefficients of the target sensor. In this paper, HJ-1 CCD cross-calibration formulas were derived and improved with MODIS as the standard sensor. Details are as follows.

Assuming that the radiometric response of HJ-1 CCD is linear, its absolute radiometric calibration formulas of top-of-atmosphere (TOA) radiance and normalized TOA reflectance (normalizing the solar zenith angle to be 0°) can be expressed as

$$\left(\frac{E_{ci}\cdot\cos\theta_{\mathrm{c}}}{\pi\cdot d^2}\cdot\rho_{\mathrm{ci}}=\right)L_{\mathrm{ci}}=DC_{ci}/a_{ci}+L_{0i},\tag{1}$$

$$(\rho_{\mathrm{ci}}\cdot\cos\theta_{\mathrm{c}}=)\ \rho^*_{ci}=DC_{\mathrm{ci}}/c_{ci}+\rho_{0i},\tag{2}$$

where L_{ci} ($\mathrm{Wm^{-2}\ sr^{-1}\ \mu m^{-1}}$) is the TOA radiance of CCD i-band; ρ_{ci} is the TOA reflectance of CCD i-band; θ_c is the solar zenith angle when CCD overpasses; ρ^*_{ci} is the normalized TOA reflectance of CCD i-band; a_{ci}, L_{0i} are the TOA radiance gain and offset of CCD i-band; c_{ci}, ρ_{0i} are the normalized TOA reflectance gain and offset of CCD i-band; DC_{ci} is the digital count value of CCD i-band; E_{ci} ($\mathrm{Wm^{-2}\ \mu m^{-1}}$) is the equivalent solar irradiance of CCD i-band at the average sun-earth distance; d^2 is the sun-earth distance correction factor at the date of CCD passing.

In addition, since the offsets of all MODIS bands are equal to zero, the MODIS normalized TOA reflectance calibration formula is

$$(\rho_{\mathrm{m}i}\cdot\cos\theta_{\mathrm{m}}=)\ \rho^*_{\mathrm{m}i}=DC_{\mathrm{m}i}\cdot c_{\mathrm{m}i},\tag{3}$$

where $\rho_{\mathrm{m}i}$ is the TOA reflectance of MODIS i-band; θ_{m} is the solar zenith angle as MODIS passes; $\rho^*_{\mathrm{m}i}$ is the normalized TOA reflectance of MODIS i-band; $DC_{\mathrm{m}i}$ is the digital count value of MODIS i-band; $c_{\mathrm{m}i}$ is the normalized TOA reflectance gain of MODIS i-band.

The cross-calibration formulas of the TOA radiance and normalized TOA reflectance for HJ-1 CCD i-band can be obtained via dividing eq. (3) by eqs. (1) and (2) respectively. They are

$$(\rho^*_{\mathrm{ci}}/\rho^*_{\mathrm{m}i})\cdot\frac{E_{ci}}{\pi\cdot d^2}\cdot DC_{\mathrm{m}i}\cdot c_{\mathrm{m}i}=DC_{ci}/a_{\mathrm{ci}}+L_{0i},\tag{4}$$

$$(\rho^*_{ci}/\rho^*_{\mathrm{m}i})\cdot DC_{\mathrm{m}i}\cdot c_{\mathrm{m}i}=DC_{\mathrm{ci}}/c_{ci}+\rho_{0i},\tag{5}$$

where $(\rho^*_{ci}/\rho^*_{\mathrm{m}i})$ is defined as spectral band matching factor. It is the ratio of two sensors' normalized TOA reflectance, which can be obtained accurately by the radiative transfer calculation and solar zenith angle normalization. It takes into account the matching of two sensors' different observation geometries and different spectral responses to surface reflectance and atmospheric parameters.

These cross-calibration formulas are improved in several aspects. (1) c_{ci} is redefined as the gain of normalized TOA reflectance, which was previously defined as the gain of TOA reflectance [13, 18]. Compared with the previous definition, the new gain is independent of solar zenith angle and thus can be used directly. (2) The definition of spectral band matching factor is developed from the ratio of TOA reflectance $(\rho_{ci}/\rho_{\mathrm{m}i})$ [13, 18, 22] to the ratio of normalized TOA reflectance $(\rho^*_{ci}/\rho^*_{\mathrm{m}i})$. The improved matching factor takes into account the matching of the solar zenith angle, and makes the formulas more concise. Additionally, the formulas' structure is also adjusted, making the fitting operation for multi-site cross-calibration more convenient and intuitive.

3 Uncertainty analysis

3.1 Uncertainty sources analysis

The sources of cross-calibration uncertainty can be listed by analyzing all the items in eqs. (4) and (5), including $(\rho^*_{ci}/\rho^*_{\mathrm{m}i})$, E_{ci}, d^2, DC_{ci}, $DC_{\mathrm{m}i}$ and $c_{\mathrm{m}i}$. Among these items, the impacts of E_{ci} and d^2 are ignored in that they can be

computed accurately. According to the other four items, the uncertainty of cross-calibration is summarized as the following three aspects.

1) Uncertainty of the standard sensor's calibration coefficient c_{mi}.

2) Pixel matching uncertainty caused by the positioning deviations while extracting DC_{mi} and DC_{ci} in MODIS and CCD images.

3) Uncertainty of spectral band matching factor (ρ^*_{ci} / ρ^*_{mi}). In order to get the accurate matching factor, it is essential to meet the following five ideal conditions during the radiative transfer calculations for the both two sensors. (I) Input precise solar zenith angle and solar azimuth for accurate atmospheric path length in incident direction. (II) Input precise view zenith angle and view azimuth for accurate atmospheric path length in the observed direction. (III) Input precise atmospheric parameters including the parameters of atmosphere component and aerosol. (IV) Input precise synchronous bidirectional reflectance under respective observation geometries. (V) Input precise field altitude needed by radiative transfer calculations. However, in actual cross-calibration process, only the first two conditions can be realized, while (III), (IV) and (V) cannot be provided easily due to the lack of synchronous data. Then, several substitution solutions are proposed. Since the acquisition times of the cross-calibration images are very close (the difference is usually less than 30 min), the same atmospheric parameters are adopted in each sensor's radiative transfer calculation. Besides, the following 5 alternative measurements are used to compensate for the lack of the synchronous data. ① Using altitude product, such as DEM or MOD03, instead of field's true value. ② Using the atmospheric component parameters obtained from the standard atmospheric model, such as water vapor content and ozone content, instead of the data obtained from synchronous measurements. ③ Using the standard aerosol model and aerosol optical thickness (AOT) product or empirical value instead of the synchronous aerosol component parameters and AOT. ④ Using historical surface spectrum or spectrum of similar ground objects instead of synchronous spectrum. ⑤ For the lack of the surface BRDF, using surface vertical reflectance instead of surface bidirectional reflectance. These alternative measurements above make the uncertain errors between input parameters and the true values, and thus bring the uncertainty of spectral band matching factor.

In summary, there are 8 sources of cross-calibration uncertainty: (1) calibration uncertainty of the standard sensor; (2) pixel matching uncertainty; (3) field altitude setting error; (4) atmospheric parameters setting error; (5) surface spectrum source; (6) surface bidirectional reflectance characteristic; (7) error of atmospheric radiative transfer model such as 6S and MODTRAN; (8) other factors which were not considered. Figure 1 shows the relationship between them.

The total uncertainty of cross-calibration is equal to the square root of the 8 uncertainties' quadratic sum [13, 18, 23]. Among them, the uncertainties of (1) and (7) are both treated as 2.0% because of the standard sensor of MODIS and the 6S radiative transfer software [18], and the uncertainty of (8) is assumed to be 1.0%. Then, the uncertainties of (2)–(6) are analyzed in detail as follows, with the required parameters shown in Table 1.

3.2 Pixel matching uncertainty

The relative location offset of the cross-calibration test site in two images is inevitable. The offset would certainly bring some error to DC_{mi} or DC_{ci}, and thereby affect the accuracy of a_{ci}, L_{0i}, c_{ci} and ρ_{0i} straightly.

The sliding window method is used to measure the error of DC_{mi} or DC_{ci}. Firstly, the site location in the image of standard sensor (or target sensor) is taken as the standard location, site location in another sensor's image as the relative location. The offset between the two locations would be a certain number of pixels. Secondly, a window at the relative location is created, the window size is determined by the size of test site. Finally, slide the window within several pixels around the relative location, thus getting the error of DC_{mi} or DC_{ci}. As the error size varies with the calibration test site, it should be specifically analyzed for each specific test-site.

3.3 Spectral band matching factor uncertainty caused by altitude setting error

For the lack of the field's measured data, alternative alti-

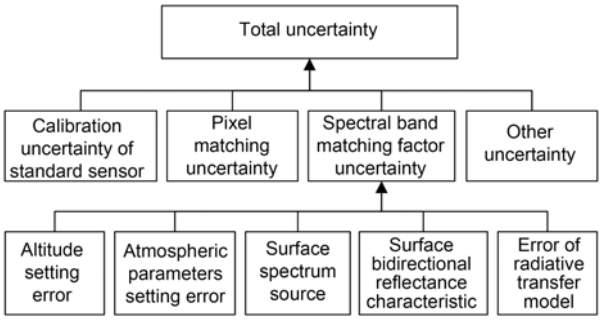

Figure 1 Sources of cross-calibration uncertainty.

Table 1 Input parameters for radiative transfer calculation

Item	Setting
Sensors	HJ-1A CCD1;MODIS
Band	1, 2, 3, 4;3, 4, 1, 2
Surface spectrum	spectrum of Dunhuang Site measured in 2010
Solar angles (°)	solar zenith angle: 30, solar azimuth: 145
View angles (°)	view zenith angle: 0, view azimuth: 0
Atmospheric model	mid-latitude summer
Aerosol model	desert type
550 nm AOT	0.15
Altitude (m)	1236

tude product is usually used to substitute the true altitude. However, there is always difference between the product and true value, resulting in a certain degree of spectral band matching factor uncertainty.

In order to analyze the impact of different altitude settings, different altitudes are seriatim input to the radiative transfer model to calculate the spectral band matching factors, while the rest parameters in Table 1 are fixed. The result is shown in Figure 2. From the result, the matching factor differences caused by 500 m altitude error are 0.21%, 0.19%, 0.08% and 0.71% on blue, green, red and near-infrared (NIR) bands, respectively; when the altitude error is 100 m, they are 0.05%, 0.05%, 0.04% and 0.17%; and then they even drop to 0.05%, 0.00%, 0.04% and 0.08% as the altitude error reduces to 50 m. Obviously, when the altitude error is less than 100 m, they are already small enough so that the uncertainty caused by the altitude setting error can be simply ignored.

3.4 Spectral band matching factor uncertainty caused by atmospheric parameters setting error

The atmospheric parameters required by radiative transfer model mainly include atmospheric component parameters and aerosol parameters. The former consists of water vapor content, ozone content, and so on; the latter is generally composed of aerosol component parameters and aerosol optical thickness. In practical cross-calibration, these parameters are commonly substituted by standard atmospheric model, standard aerosol model, and empirical AOT or MOD04 product. These substitutions are bound to make atmospheric parameters errors, and thereby bring a certain degree of spectral band matching factor uncertainty.

In order to analyze the impact of these substitutions, keeping the rest parameters in Table 1 unchanged, different atmospheric parameters are input to the radiative transfer model in sequence to calculate the spectral band matching factors. Firstly, the influence of atmospheric component parameters setting can be obtained by changing water vapor content (g cm^{-2}) from 0.5 to 3.5 with an interval of 0.5 and ozone content (cm-atm) from 0.25 to 0.45 with an interval of 0.02. The result is shown in Figure 3. Secondly, the influence of aerosol parameters setting can be obtained by changing aerosol model from desert type to continental type (this is because that the aerosol model of Dunhuang Calibration Site is between continental type and desert type [24]) and AOT from 0.05 to 0.55 with an interval of 0.05, and the result is shown in Figure 4.

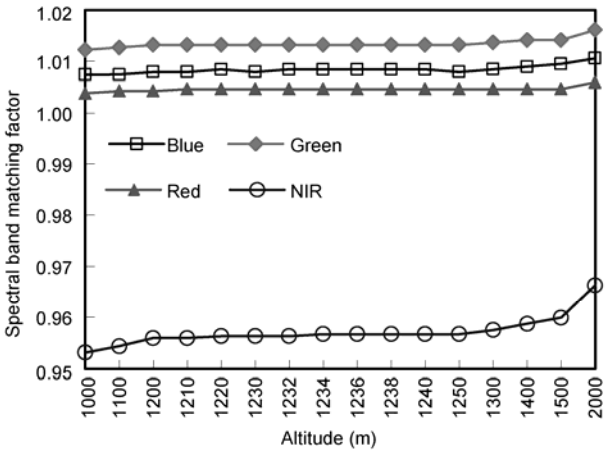

Figure 2 Influence caused by the setting of altitude.

Figure 3 shows that, the biggest differences of spectral band matching factor caused by the setting of ozone content within 0.25–0.45 are 0.59%, 0.28%, 0.83% and 0.04% on each band, and the biggest differences caused by the setting of water vapor content within 0.5–3.5 are 0.15%, 0.75%, 0.21% and 3.46%. Figure 4 shows that the biggest differences caused by the setting of 550 nm AOT within 0.05–0.55 are 1.15%, 0.29%, 0.16% and 0.16%, and the biggest differences caused by the setting of desert type aerosol or continental type aerosol are 0.44%, 0.05%, 0.20% and 0.24%. It is obvious that the uncertainties caused by the setting of ozone content, water vapor content, aerosol model, and AOT are all very small, so the substitutions mentioned above are feasible.

3.5 Spectral band matching factor uncertainty caused by surface spectrum source

Normally, historical surface spectrum or spectrum of similar ground feature is used to compensate for the lack of the synchronous surface reflectance [13, 18], thus bringing some spectral band matching factor uncertainty.

Firstly, 13 historical surface spectra are used to analyze the influence caused by the substitution of historical surface spectrum. These spectra, which were acquired in Dunhuang Calibration Site during 1999–2010, are input to the radiative transfer model in sequence to calculate the spectral band matching factors, keeping the rest parameters in Table 1 unchanged, and the result is shown in Figure 5. The matching factor differences on each band are 0.75%, 0.85%, 0.34% and 0.44% respectively. The differences are small, and therefore it is feasible to use historical surface spectrum to replace the synchronous surface spectrum in cross-calibration.

Secondly, 33 spectra selected from 5 types of features are used to analyze the influence caused by the substitution of spectrum of similar ground feature. These spectra, which are mainly taken from the *Spectral Data Sets for Satellite Calibration Site and Typical Earth Objects* [25] (hereinafter referred to as *Data Sets*) and ENVI Spectral Library, consist of 6 sandy ground spectra, 6 water spectra, 9 soil spectra, 5 snow spectra and 7 tree crown spectra. They are seriatim imported into the radiative transfer model to calculate the spectral band matching factors with the rest of the parameters in Table 1 fixed, and the result is shown in Figure 6. Seen from Figure 6, the matching fac-

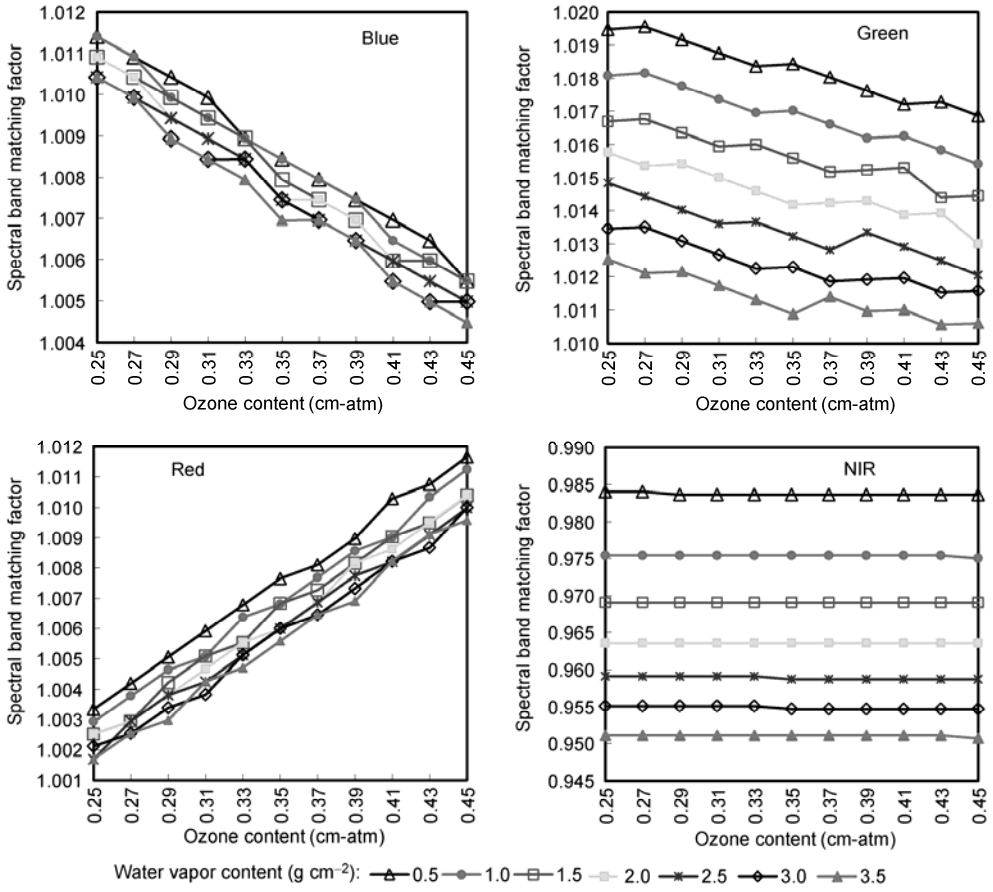

Figure 3 Influence of the atmospheric component parameters.

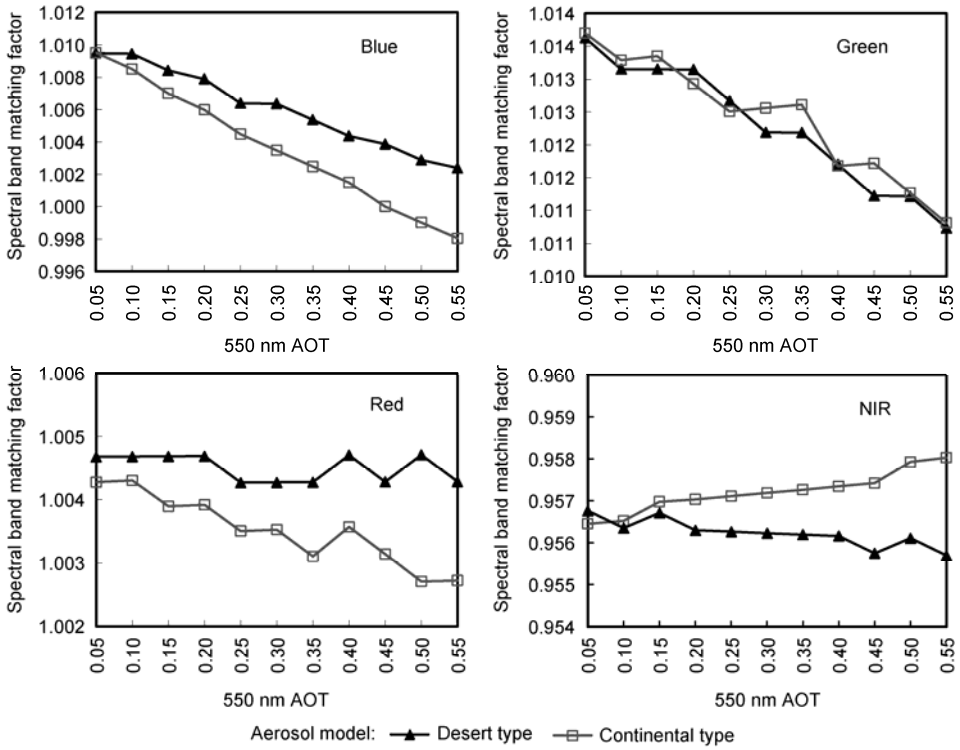

Figure 4 Influence of aerosol parameters.

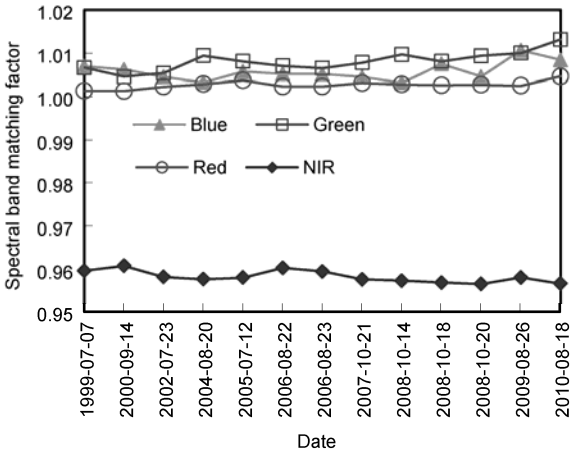

Figure 5 Influence of substitution of historical surface spectrum.

tor differences between different sandy grounds on each band are small, especially for the snow grounds. The former are 3.09%, 1.59%, 1.18% and 1.91%, and the latter are 0.22%, 0.15%, 0.62% and 1.71%. Among different soils, the matching factor differences on each band are large in general. They are 6.91%, 3.20%, 2.29% and 3.02%, but they will become very small after these soils are divided into two categories of silty soil and sandy soil. The differences are only 1.30%, 0.91%, 0.94% and 1.57% for silty soil, and only 1.68%, 1.27%, 2.29% and 0.87% for sandy soil. However, among different water bodies, the matching factor differences are very large. They are all greater than 6.0% on each band, and especially on the near-infrared band, the difference is as high as 17.66%. This could be caused by the water quality and its nature of low SNR. Additionally, the matching factor differences among different tree

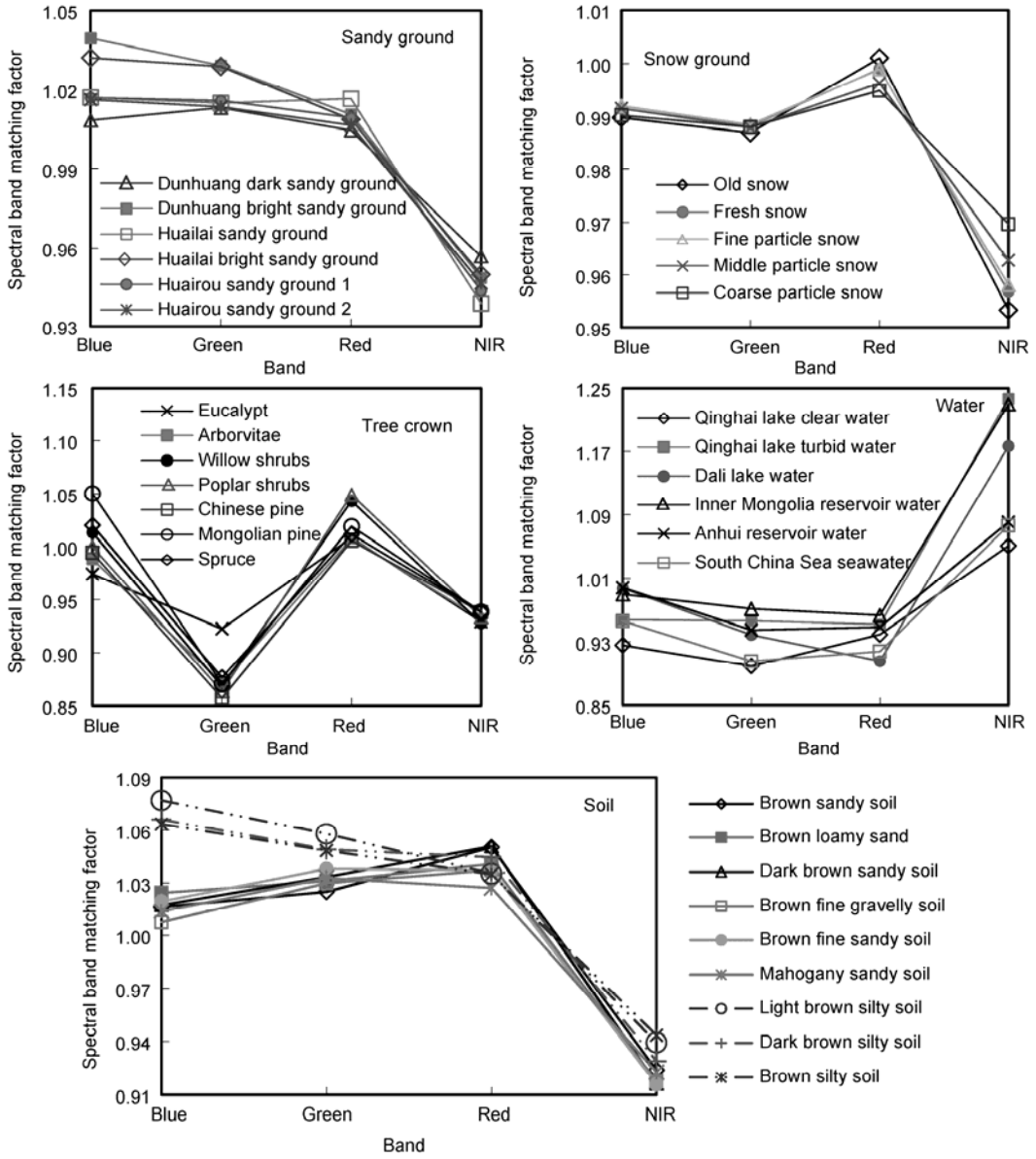

Figure 6 Influence caused by the substitution of spectrum of similar ground feature.

crowns vary with the actual tree species. In conclusion, when the spectrum of similar ground feature is needed by the cross-calibration for the lack of the synchronous surface reflectance, the concrete type of surface feature should be taken into account, but not all feature types are suitable for this substitution.

3.6 Spectral band matching factor uncertainty caused by surface bidirectional reflectance characteristic

Most of the natural surfaces are not Lambert, and the BRDF is commonly used to describe this bidirectional reflectance characteristic. However, due to the lack of the surface BRDF, in cross-calibration, surface vertical reflectance is usually used to substitute the bidirectional reflectance. In order to analyze the spectral band matching factor uncertainty caused by this substitution, firstly, the exact spectral band matching factor is calculated by using the surface bidirectional reflectance in radiative transfer model. Then, the alternative matching factor is calculated by substituting the surface vertical reflectance for the bidirectional reflectance. Finally, alternative factor and exact factor are compared, thereby obtaining the uncertainty caused by surface bidirectional reflectance characteristic. In the analysis, since the difference of acquisition time of the image pair is generally within 30 min, the difference of solar zenith angle is not considered, and only the influences of view zenith angle and scattering angle (the difference between the view azimuth and solar azimuth) need to be considered.

The required data come from the *Data Sets*, including the surface reflectance of Dunhuang Site measured on September 4, 2000 which cover the range of view zenith angle from 50° forward to 50° backward in 5° step on the solar principal plane, and the surface reflectance measured on July 7 and 17, 1999 with the coverage of view zenith angle from 5.4° to 54° in 5.4° step and scattering angle from –230° to +20° in 5° step. The former was acquired in the location of (40°05′00″N, 94°23′00″E) at about Beijing Time 13:50 when the solar zenith angle was 33.04° and the solar azimuth was 183.88°. The latter is located on (40°05′24″N, 94°24′00″E) and was measured at about 12:00 when the solar zenith angle was 28.50° and the solar azimuth was 119.53°.

3.6.1 Influence of substituting vertical reflectance for bidirectional reflectance in different view zenith angles

The spectral band matching factor difference caused by substituting vertical reflectance for bidirectional reflectance in respective view zenith angles of the two sensors is analyzed by using the spectral data measured on September 4, 2000. Firstly, solar zenith angle is set as 33.04°, solar azimuth is set as 183.88°, view zenith angle of HJ-1A CCD1 is changed from 30° forward to 30° backward in 5° step, view zenith angle of MODIS is changed from 50° forward to 50° backward in 5° step, and then the bidirectional reflectance in the corresponding view zenith angles are input to radiative transfer model in sequence with the other parameters in Table 1 unchanged to calculate the exact factor. Secondly, the surface reflectance in 0° view zenith angle is used to substitute each bidirectional reflectance and calculate the alternative factor. At last, the error is got by comparing the alternative factor with exact factor. According to the result shown in Figure 7, the following conclusions can be obtained.

1) In general, the errors of alternative factors on the solar principal plane are very large. The maximal errors on each band are as high as 12.08%, 16.30%, 17.71% and 18.49% respectively. And it is more serious in backward directions than forward. In backward directions, more than half of the errors are greater than 5%, and more than 15% of the errors are greater than 10%. Even though in forward directions, the maximal errors on each band are also as high as 3.98%, 6.07%, 7.49% and 6.93% respectively. Therefore, it is not very applicable to substituting vertical reflectance for bidirectional reflectance without considering the actual view zenith angle.

2) When the view zenith angles of the two sensors are the same on the solar principal plane, the errors of the alternative spectral band matching factors are all the smallest and the maximal errors on each band are only 0.49%, 0.11%, 0.07%% and 0.29%. Thus, if there is a pair of images like this, it will be very ideal and provides a new way for high precise cross-calibration.

3) When the difference of the two sensors' view zenith angles is less than 5° on the solar principal plane, the maximal errors in forward directions on each band are only 1.01%, 1.26%, 1.48% and 1.52%, they are also 2.58%, 2.71%, 2.79% and 3.03% in backward directions. The errors are small and acceptable.

4) In summary, in the case that the two sensors are both on the solar principal plane, the view zenith angles of the image pair should be consistent or with a difference of less than 5°,or else the surface BRDF should be taken into account. The case that the sensors are not on the solar principal plane is discussed in detail in Section 3.6.3.

3.6.2 Influence of substituting vertical reflectance for bidirectional reflectance in different scattering angles

The difference of spectral band matching factors caused by substituting vertical reflectance for bidirectional reflectance in respective scattering angles of the two sensors is analyzed by using the spectral data in 5.4° view zenith angle measured on July 7, 1999. Firstly, solar zenith angle is set as 28.50°, solar azimuth is set as 119.53°, view zenith angle is set as 5.4°, view azimuth of CCD1 and MODIS are reduced severely from 119.53° to –60.47° in 30° step, and then the bidirectional reflectance in corresponding scattering angles are input to radiative transfer model to calculate the exact factor. Secondly, the alternative factor

is calculated by using the surface vertical reflectance instead of each bidirectional reflectance. Finally, the error is obtained by comparing the alternative factor with exact factor. The results are shown in Figure 8.

As shown in Figure 8, there is no evident regularity of this replacement influence. In the 5.4° view zenith angle, the maximal errors on each band are 4.86%, 4.28%, 5.13% and 5.53% respectively, which are relatively large. These errors will bring cross-calibration a big uncertainty. Nevertheless, it can be found that when the scattering angles of the two sensors are the same, the errors of the alternative spectral band matching factors are all very small with the maximal errors on each band being only 0.38%, 0.30%, 0.12% and 0.11% respectively.

3.6.3 Spectral band matching factor uncertainty under the same observation geometry

According to the analysis in Sections 3.6.1 and 3.6.2, under most observation geometries, the substitution of surface vertical reflectance for bidirectional reflectance would

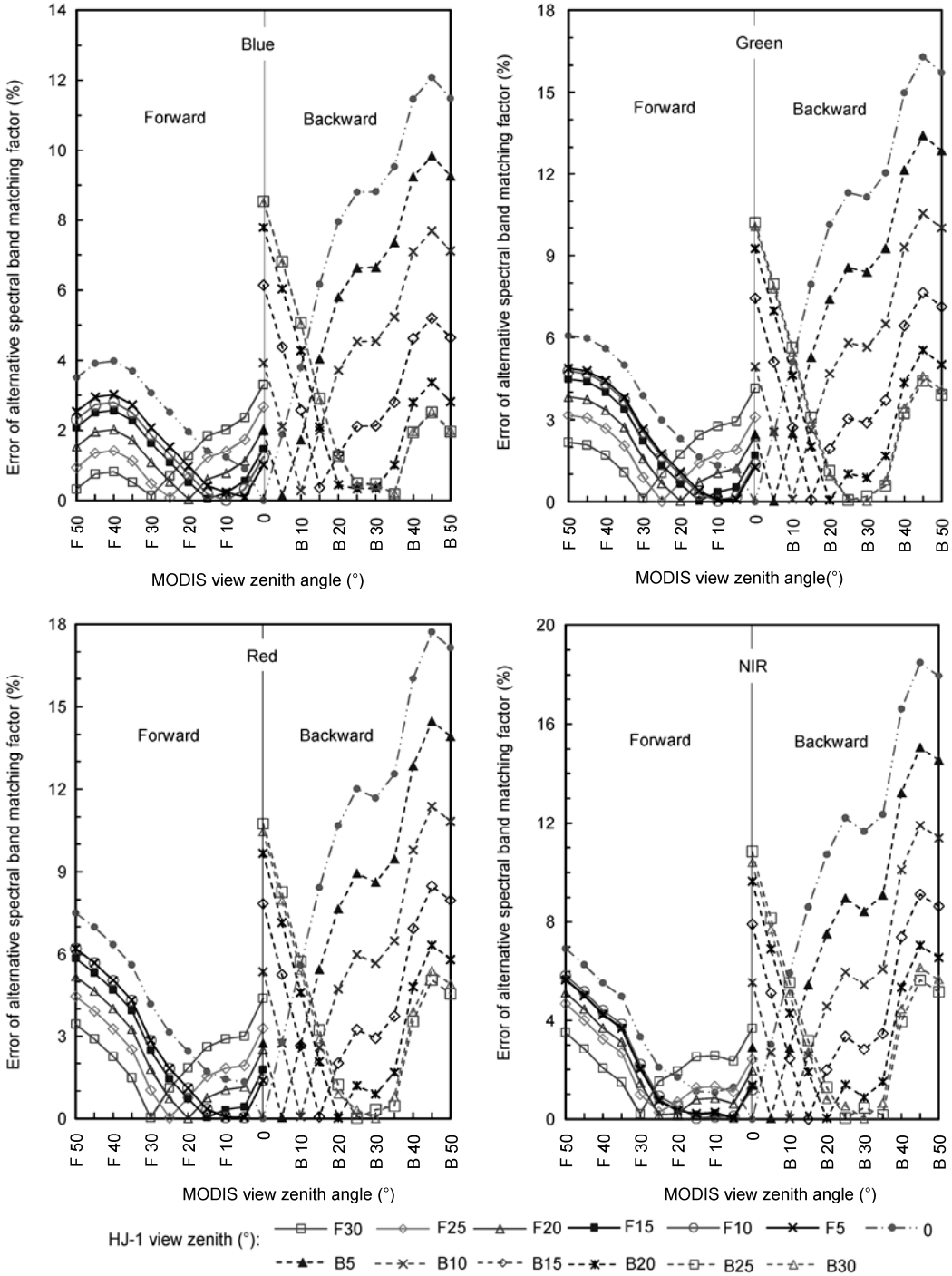

Figure 7 Influenceof view zenith angle (F: Forward; B: Backward).

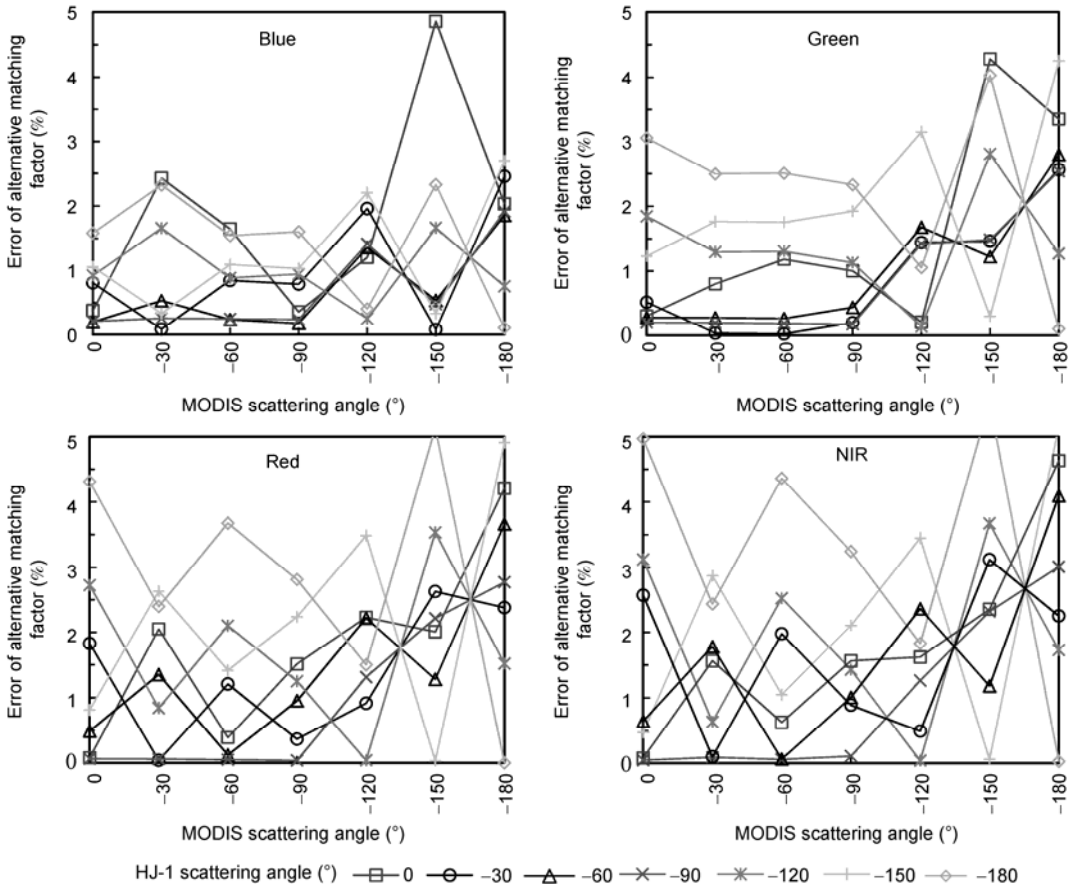

Figure 8 Influence of scattering angle.

make great uncertainty to cross-calibration. However, in some special angles, the uncertainty caused by this alternative measurement is very small. Section 3.6.1 indicates that the uncertainty is no more than 0.5% when the view zenith angles of the two sensors are the same on the solar principal plane. Section 3.6.2 also shows that the uncertainty is less than 0.4% when the two sensors' scattering angles are the same and the view zenith angles are both 5.4°. Just imagine: within the whole hemisphere space, if two sensors have consistent zenith angle and scattering angle, is the uncertainty of this substitution still small? If so, how much is the specific value?

In order to analyze the spectral band matching factor uncertainty caused by substitution of surface vertical reflectance for bidirectional reflectance in the same observation geometry of the two sensors, the spectral data measured on July 7 and 17, 1999 are used. Firstly, solar zenith angle is set as 28.50°, solar azimuth is set as 119.53°, two sensors' view zenith angles are changed synchronously from 5.4° to 32.4° in 5.4° step, scattering angles of the two sensors are also reduced synchronously from 0° to −180° in 10° step. Then, the corresponding bidirectional reflectance data are imported into radiative transfer model to calculate the exact factor. At last, the alternative factor is calculated by using the surface vertical reflectance. The result is shown in Figure 9.

As shown in Figure 9, when the two sensors have consistent zenith angle and scattering angle within the whole scope of hemisphere space, the differences between the exact value and alternative value of spectral band matching factor in each band are all very small. The maximal errors in each band are only 0.898%, 0.917%, 0.323% and 0.282%. That is, when the observation geometries of the two sensors are consistent, it is completely feasible by substituting surface vertical reflectance for bidirectional reflectance to calculate the spectral matching factor and obtain high precise cross-calibration coefficients.

4 Conclusions and prospect

In this paper, cross-calibration formulas were improved by redefining calibration coefficient and spectral band matching factor, and the sources of cross-calibration uncertainty were proposed by contrasting the ideal and actual conditions in cross-calibration, then the contributions of each uncertainty were further analyzed and discussed for HJ-1 CCD. The main conclusions are shown as follows. (1) The im-

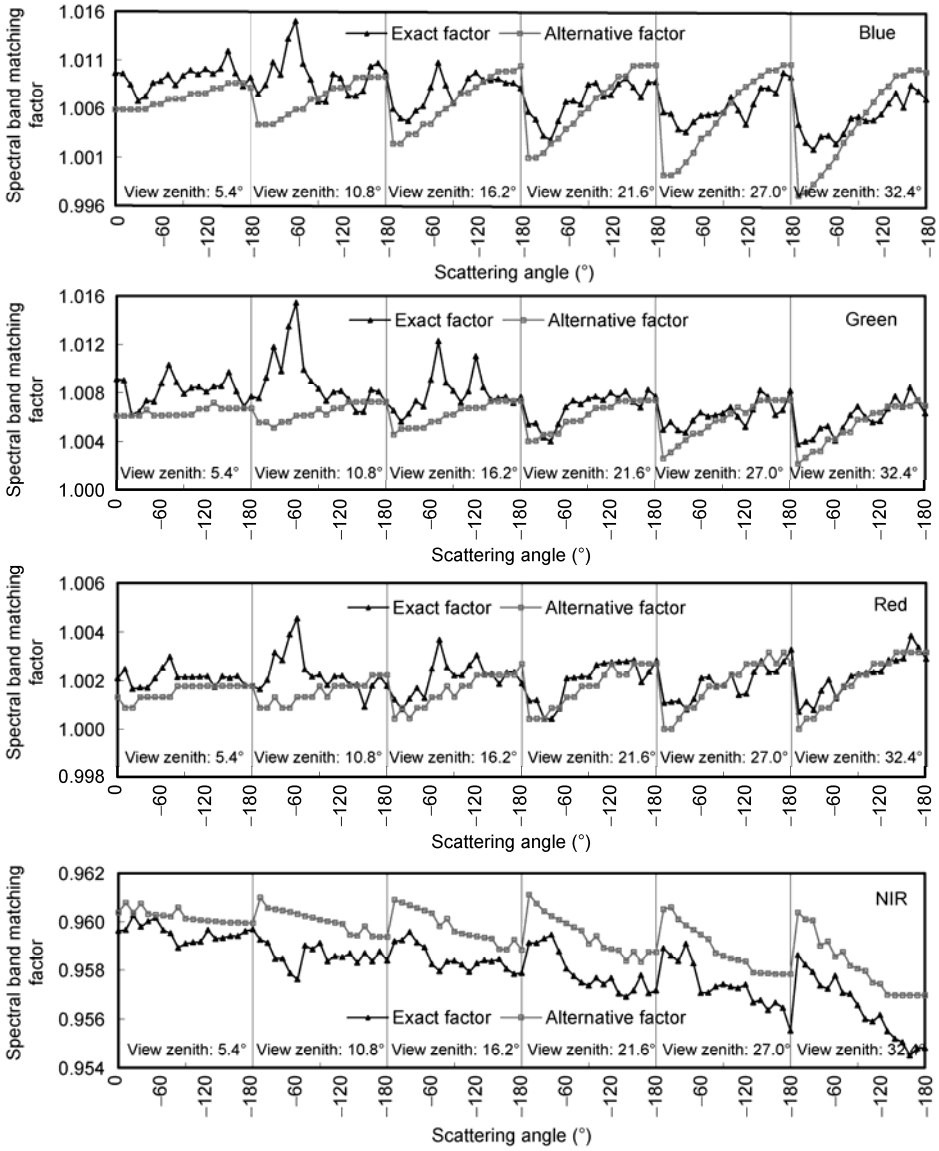

Figure 9 Spectral band matching factor under the same observation geometry.

Table 2 Summary of the source, size and approach of the cross-calibration uncertainty

No.	Source			Size	Approach
1	calibration uncertainty of the standard sensor			2%	counted in total uncertainty
2	pixel matching uncertainty			vary with the test site	sliding window analysis
3	altitude setting error			extremely small	ignored
4	atmospheric parameters setting error	4-1	ozone content setting error	bands 1, 2, 3: <1% band 4: extremely small	bands 1, 2, 3: counted in total uncertainty band 4: ignored
		4-2	water vapor content setting error	bands 1, 2, 3: <1% band 4: 3.46%	counted in total uncertainty
		4-3	aerosol component setting error	bands 1, 3, 4: <1% band 2: extremely small	bands 1, 3, 4: counted in total uncertainty band 2: ignored
		4-4	AOT setting error	<1.2%	counted in total uncertainty
5	surface spectrum source	5-1	historical surface spectrum	<1%	counted in total uncertainty
		5-2	spectrum of similar ground feature	vary with ground feature	snow, sand can be considered
6	surface bidirectional reflectance characteristic			very large	reflectance correction by using BRDF or choose the image pair with coincident observation geometry
7	error of atmospheric radiative transfer model			2%	counted in total uncertainty
8	other factors which were not considered			1%	counted in total uncertainty

proved cross-calibration formulas take solar zenith angle into consideration, so the result of cross-calibration can be issued to users directly. (2) There are 8 sources of cross-calibration uncertainty, which are shown in Table 2. (3) The difference between the contributions of these sources is large, the specific contributions and processing methods are presented in Table 2. Among these uncertainty sources, surface bidirectional reflectance characteristic has the greatest influence on spectral band matching factor, so it is not an applicable measurement to substitute vertical reflectance for bidirectional reflectance without considering the actual view zenith angle. It is very important to correct reflectance by using surface BRDF or choose the image pair with coincident observation geometry in cross-calibration. Besides, the concrete type of surface feature should be taken into account, but not all the feature type can be substituted by the similar ground feature.

Uncertainty analysis of cross-calibration provides many valuable references for evaluating the feasibility of alternative cross-calibration measurements. The next step is to execute the cross-calibration for HJ-1 CCD by choosing appropriate image pairs and alternative measurements, thus the high accuracy calibration coefficients can be obtained.

This work was supported by the Chinese Defence Advance Research Program of Science and Technology (Grant No. 07K00100KJ), the National High Technology Research and Development Program of China ("863"Project) (Grant No. 2006AA12Z113), the International Science and Technology Cooperation Program of China (Grant No. 2008DFA21540), and A Project Funded by the Priority Academic Program Development of Jiangsu Higher Education Institutions (PAPD).

1 Brest C L, Rossow W L. Radiometric calibration and monitoring of NOAA AVHRR data for ISCCP. Int J Remote Sens, 1992, 13(2): 235–273
2 Rao C R N, Chen J. Inter-satellite calibration linkages for the visible and near-infared channels of the Advanced Very High Resolution Radiometer on the NOAA-7, -9, and-11 spacecraft. Int J Remote Sens, 1995, 16(11): 1931–1942
3 Henry P, Meygret A. Calibration of HRVIR and vegetation cameras on SPOT4. Adv Space Res, 2001, 28(1): 49–58
4 Teillet P M, Barker J L, Markham B L, et al. Radiometric cross-calibration of the Landsat-7 ETM+ and Landsat-5 TM sensors based on tandem data sets. Remote Sens Environ, 2001, 78(1-2): 39–54
5 Scott K P. Radiometric calibration of on-orbit satellite sensors using an improved cross-calibration method. Doctoral Dissertation. Tucson: The University of Arizona, 1998. 73–134
6 Eplee R E, Sun J Q, Meister G, et al. Cross calibration of SeaWiFS and MODIS using on-orbit observations of the Moon. Appl Optics, 2011, 50(2): 120–133
7 Arai K. Inflight test site cross calibration between mission instruments onboard the same platform. Adv Space Res, 1997, 19(9): 1317–1324
8 Rao C R N, Cao C, Zhang N. Inter-calibration of the Moderate-Resolution Imaging Spectroradiometer and the Along Track Scanning Radiometer-2. Int J Remote Sens, 2003, 24(9): 1913–1924
9 Schroeder M, Poutier L, Muller R, et al. Intercalibration of optical satellites—A case study with MOMS and SPOT. Aerosp Sci Technol, 2001, 5(4): 305–315
10 Teillet P M, Fedosejevs G, Gauthier R P, et al. A generalized approach to the vicarious calibration of multiple Earth observation sensors using hyperspectral data. Remote Sens Environ, 2001, 77(3): 304–327
11 Hagolle O, Goloub P, Deschamps P Y, et al. Results of POLDER in-flight calibration. IEEE T Geosci Remote, 1999, 37(3): 1550–1566
12 Yang Z D, Gu S Y, Qiu H, et al. CBERS-1's CCD image quality evaluating and cross calibrating study (in Chinese). J Remote Sens, 2004, 8(2): 113–115
13 Li X Y, Gu X F, Min X J, et al. Radiometric cross-calibration of the CBERS-02CCD camera with the TERRA MODIS. Sci China Ser E-Tech Sci, 2005, 48(Suppl I): 44–60
14 Tang J W, Gu X F, Niu S L, et al.Water target based cross-calibration ofCBERS-02 CCD camera with MODIS data. Sci China Ser E-Tech Sci, 2005, 48(Supp I): 61–71
15 Cheng Z C, Liu X, Li J S, et al. The cross calibration of Beijing-1 Microsatellite Multispectral Sensors (in Chinese). J Astronaut, 2008, 29(2): 637–643
16 Tong J J. The study on synthesis radiometric calibration methods for satellite sensors (in Chinese). Doctoral Dissertation. Beijing: Beijing Normal University, 2004. 48–68
17 Hu X Q, Liu J J, Qiu K M, et al. New method study of sites vicarious calibration for SZ-3/CMODIS (in Chinese). Spectrosc Spect Anal, 2009, 29(5): 1153–1159
18 Gong H. Study on the Calibration and validation of CCD Camera on HJ-1 Satellites (in Chinese). Doctoral Dissertation. Beijing: Institute of Remote Sensing Applications of Chinese Academy of Sciences, 2010. 51–91
19 Xu L, Ma L L, Hu J, et al. Cross-calibration of HJ-1B/CCD1 against Terra/MODIS (in Chinese). Remote Sens Inf, 2011, (02): 26–31
20 Yu X L, Wu Z C. The comparison between HJ Satellite's CCD sensors field calibration and cross calibration (in Chinese). Chin J Sens Actu, 2011, 24(10): 1435–1439
21 Pan D L, He X Q, Zhu Q K. In-orbit cross-calibration of HY-1A satellite sensor COCTS. Chin Sci Bull, 2004, 49(21): 2521–2526
22 Teillet P M, Fedosejevs G, Thome K J, et al. Impacts of spectral band difference effects on radiometric cross-calibration between satellite sensors in the solar-reflective spectral domain. Remote Sens Environ, 2007, 110(3): 393–409
23 Gao H L, Gu X F, Yu T, et al. Radiometric calibration for HJ-1A Hyper-Spectrum Imager and uncertainty analysis (in Chinese). Acta Photon Sin, 2009, 38(11): 2826–2833
24 Hu X Q, Zhang Y X, Zhang G S, et al. Measurement and study ofaerosol optical characteristics in China radiometric calibration sites (inChinese). J Appl Meteorol Sci, 2001, 12(3): 257–266
25 China Radiometric Calibration Site of Remote Sensing Satellite, Key Laboratory of Radiometric Calibration and Validation for Environmental Satellites of China Meteorological Administration. Spectral Data Sets for Satellite Calibration Site and Typical Earth Objects (in Chinese). Beijing: China Meteorological Press, 2008. 1–346